Sensitivity Analysis

Oliwer Sliczniuk[a,*], Pekka Oinas[a]

[a]Aalto University, School of Chemical Engineering, Espoo, 02150, Finland

ARTICLE INFO

Keywords:
Supercritical extraction
Sensitivity analysis
Mathematical modelling

ABSTRACT

This study investigates the process of chamomile oil extraction from chamomile flowers. A parameter-distributed model, consisting of a set of partial differential equations, is used to describe the governing mass transfer phenomena between solid and fluid phases under supercritical conditions using carbon dioxide as the solvent. The concept of quasi-one-dimensional flow is applied to reduce the number of spatial dimensions. The flow is assumed to be uniform across any cross-section, although the area available for the fluid phase can vary along the extractor. The physical properties of the solvent are estimated using the Peng-Robinson equation of state. Laboratory experiments were conducted under various, but constant operating conditions: $30-40°C$, $100-200$ bar, and $3.33-6.67\cdot10^{-5}$ kg/s. Different sensitivity analysis methods can be applied to assess the robustness of the model parameters and their influence on the process model. Local sensitivity analysis investigates the impact of infinitesimally small changes in model parameters and controls on model output. This study focuses on analysing the effect of pressure on the model state space and extraction yield.

1. Introduction

This study investigates the extraction of essential oil from chamomile flowers (Matricaria chamomilla L.) via supercritical fluid extraction techniques and the modelling of this process. Chamomile is a medicinal herb widely cultivated in southern and eastern Europe in countries such as Germany, Hungary, France and Russia. It can be found outside Europe, for instance in Brazil as discussed by Singh et al. [1]. This plant is distinguished by its hollow, bright gold cones, housing disc or tubular florets and surrounded by about fifteen white ray or ligulate florets. Chamomile has been used for its medicinal benefits, serving as an anti-inflammatory, antioxidant, mild astringent, and healing remedy. Aqueous extract of chamomile is widely used to calm nerves and mitigate anxiety, hysteria, nightmares, insomnia and other sleep-related conditions, according to Srivastava [2]. Orav et al. [3] reported that oil yields from dried chamomile samples ranged from 0.7 to 6.7 mL/kg. The highest yields of essential oil, between 6.1 and 6.7 mL/kg, were derived from chamomile sourced from Latvia and Ukraine. In comparison, chamomile from Armenia exhibited a lower oil content of 0.7 mL/kg.

Evaluating the economic viability of the process is essential when choosing a suitable technology for essential oil extraction. Traditional methods, such as distillation and organic solvent extraction, are commonly employed but have drawbacks. Distillation, for example, involves high temperatures that can lead to the thermal degradation of heat-sensitive compounds. This limitation has led to the increased popularity of alternative techniques such as supercritical fluid extraction. Supercritical carbon dioxide is appealing thanks to its distinctive properties: it is inflammable, non-toxic and non-corrosive. Supercritical fluids can exhibit both gas- and liquid-like properties, allowing for adjustable dissolving power through changes in operating conditions.

The literature offers various mathematical models to describe the extraction of valuable compounds from biomass. Selecting a process model is case-to-case dependent and requires analysis of each model's specific assumptions about mass transfer and thermodynamic equilibrium.

The model proposed by Reverchon et al. [4] is called the hot ball model, as it is based on an analogy to heat transfer and describes an extraction process from solid particles. This model assumes that particles contain low quantities of solute and that solubility is not a limiting factor.

The Broken-and-Intact Cell model, proposed by Sovova [5], assumes that external surfaces of particles are mechanically disrupted, allowing the solvent access to the solute in the broken cells. In contrast, the solute in intact cells remains less accessible due to higher mass transfer resistance.

Reverchon [6] formulated a fluid-solid extraction model where the solute is treated as a single component, governed by internal mass transfer resistance and omitting the effects of external mass transfer, axial dispersion and variations in fluid density and flow rate throughout the bed.

This work builds upon the linear kinetic model suggested by Reverchon [6], deriving fundamental governing equations to develop a comprehensive model for the chamomile oil extraction process. This model aims for control-oriented simplicity, assuming a semi-continuous operation within a cylindrical vessel. The process involves a supercritical solvent being pumped through a fixed bed of finely chopped biomass to extract the solute, followed by separation of the solvent and solute in a flush drum to collect the extract. Parameters such as pressure (P), feed flow rate (F_{in}) and inlet temperature (T_{in}) are adjustable and measurable, while the outlet temperature (T_{out}) and the amount of product at the outlet can only be monitored. Figure 1 presents a simplified process flow diagram.

This study aims to analyze the influence of changes in operating conditions on the process model described

*Corresponding author

oliwer.sliczniuk@aalto.fi (O. Sliczniuk)

ORCID(s): 0000-0003-2593-5956 (O. Sliczniuk); 0000-0002-0183-5558 (P. Oinas)

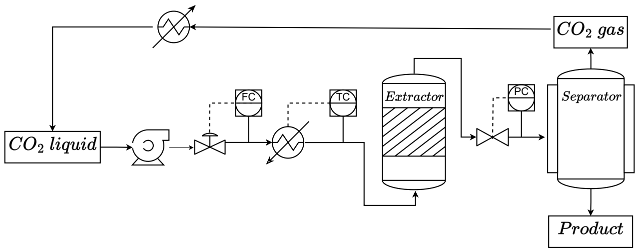

Figure 1: Process flow diagram

in article 1. Sensitivity analysis is applied to examine the impact of model parameters or controls on the model output. The results of sensitivity analysis can be used to identify sources of uncertainty, simplify the model, or detect errors by revealing unexpected relationships between inputs and outputs. Various sensitivity analysis methods are available, including:

- One-at-a-time method
- Derivative-based local methods
- Variance-based methods

Different supercritical extraction models have been analyzed using various sensitivity analysis techniques in the literature. For instance, Fiori et al. [7] performed sensitivity calculations by varying parameters within their confidence intervals and observing the changes in model results. Their analysis revealed that particle diameter and internal mass transfer coefficient significantly influence extraction during the diffusion-control regime.

Santos et al. [8] considered the model of Sovova [5] for semi-continuous isothermal and isobaric extraction processes using carbon dioxide as a solvent. They conducted a parametric sensitivity analysis using a two-level factorial design, disturbing model parameters by 10% and analyzing their main effects. They proposed strategies for high-performance operation based on sensitivities related to superficial velocity, particle diameter, initial solute concentration in the solid phase, and solute concentration in the fluid phase at the extractor inlet.

Hatami and Ciftci [9] performed a one-factor-at-a-time sensitivity analysis to assess the response of net present value to variations in technical and economic variables. Their study consists of two parts. The first part examines how net present value is influenced by changes in individual technical and economic parameters, keeping the extractor volume constant at 300 L. The second part investigates the effects of varying the extractor volume (from 1 to 600 L) on the project's overall profitability. Their findings indicate that the most influential factors on net present value include the price of the extract, interest rate, dynamic time, and project lifetime.

2. Materials and methods

2.1. Governing equations

Following the work of Anderson [10], the governing equations for a quasi-one-dimensional flow were derived. A quasi-one-dimensional flow refers to a fluid flow scenario assuming that the flow properties are uniformly distributed across any cross-section. This simplification is typically applied when the flow channel's cross-sectional area changes, such as through irregular shapes or partial filling of an extractor. According to this assumption, velocity and other flow properties change solely in the flow direction.

As discussed by Anderson [11], all flows are compressible, but some of them can be treated as incompressible when the Mach number is smaller than 0.3. This assumption leads to the incompressible condition: $\nabla \cdot u = 0$, which is valid for constant density (strict incompressible) or varying density flow. The assumption allows for removing acoustic waves and large perturbations in density and/or temperature. In the 1-D case, the incompressibility condition becomes $\frac{du}{dz} = 0$, so the fluid velocity is constant.

The set of quasi-one-dimensional governing equations in Cartesian coordinates is described by Equations 1 - 3:

$$\frac{\partial \left(\rho_f A_f\right)}{\partial t} + \frac{\partial \left(\rho_f A_f v\right)}{\partial z} = 0 \tag{1}$$

$$\frac{\partial \left(\rho_f v A_f\right)}{\partial t} + \frac{\partial \left(\rho_f A_f v^2\right)}{\partial z} = -A_f \frac{\partial P}{\partial z} \tag{2}$$

$$\frac{\partial \left(\rho_f e A_f\right)}{\partial t} + \frac{\partial \left(\rho_f A_f v e\right)}{\partial z} = -P \frac{\left(A_f v\right)}{\partial z} + \frac{\partial}{\partial z}\left(k \frac{\partial T}{\partial z}\right) \tag{3}$$

where ρ_f is the density of the fluid, A_f is the function which describes a change in the cross-section, v is the velocity, P is the total pressure, e is the internal energy of the fluid, t is time and z is the spatial direction.

2.2. Extraction model

2.2.1. Continuity equation

The previously derived quasi-one-dimensional continuity equation (Equation 1) is redefined by incorporating the function $A_f = A\phi$. This modification distinguishes constant and varying terms, where the varying term accounts for changes in the cross-sectional area available for the fluid. Equation 4 shows the modified continuity equation:

$$\frac{\partial(\rho_f \phi)}{\partial t} + \frac{\partial(\rho_f v A \phi)}{\partial z} = 0 \tag{4}$$

where A is the total cross-section of the extractor and ϕ describes porosity along the extractor.

Assuming that the mass flow rate is constant in time, the temporal derivative becomes the mass flux F, and the spatial derivative can be integrated along z as

$$\int \frac{\partial(\rho_f v A \phi)}{\partial z} dz = F \rightarrow F = \rho_f v A \phi \tag{5}$$

To simplify the system dynamics, it is assumed that F is a control variable and affects the whole system instantaneously (due to $\nabla \cdot u = 0$), which allows finding the velocity profile that satisfies mass continuity based on F, ϕ and ρ_f:

$$v = \frac{F}{\rho_f A \phi} \tag{6}$$

Similarly, superficial velocity may be introduced:

$$u = v\phi = \frac{F}{\rho_f A} \tag{7}$$

The fluid density ρ_f can be obtained from the Peng-Robinson equation of state if the temperature and thermodynamic pressure are known along z. Variation in fluid density may occur due to pressure or inlet temperature changes. In a non-isothermal case, in Equations 6 and 7 ρ_f is considered the average fluid density along the extraction column.

2.2.2. Mass balance for the fluid phase

Equation 8 describes the movement of the solute in the system, which is constrained to the axial direction due to the quasi-one-dimensional assumption. Given that the solute concentration in the solvent is negligible, the fluid phase is described as pseudo-homogeneous, with properties identical to those of the solvent itself. It is also assumed that the thermodynamic pressure remains constant throughout the device. The analysis further simplifies the flow dynamics by disregarding the boundary layer near the extractor's inner wall. This leads to a uniform velocity profile across any cross-section perpendicular to the axial direction. Thus, the mass balance equation includes convection, diffusion and kinetic terms representing the fluid phase behaviour:

$$\frac{\partial c_f}{\partial t} + \frac{1}{\phi}\frac{\partial \left(c_f u\right)}{\partial z} = \frac{1-\phi}{\phi} r_e + \frac{1}{\phi}\frac{\partial}{\partial z}\left(D_e^M \frac{\partial c_f}{\partial z}\right) \tag{8}$$

where c_f represents the solute concentration in the fluid phase, r_e is the mass transfer kinetic term and D_e^M is the axial diffusion coefficient.

2.2.3. Mass balance for the solid phase

As given by Equation 9, the solid phase is considered stationary, without convection and diffusion terms in the mass balance equation. Therefore, the only significant term in this equation is the kinetic term of Equation 10, which connects the solid and fluid phases. For simplicity, the extract is represented by a single pseudo-component:

$$\frac{\partial c_s}{\partial t} = \underbrace{r_e}_{\text{Kinetics}} \tag{9}$$

2.2.4. Kinetic term

As the solvent flows through the bed, CO_2 molecules diffuse into the pores and adsorb on the particle surface to form an external fluid film around the solid particles due to the solvent-solid matrix interactions. The dissolved solute diffuses from the particle's core through the solid-fluid interface, the pore and the film into the bulk. Figure 2 shows the mass transfer mechanism, where the mean solute concentration in the solid phase is denoted as c_s, and the equilibrium concentrations at the solid-fluid interface are denoted as c_s^* and c_p^* for the solid and fluid phases, respectively. The concentration of the solutes in the fluid phase in the centre of the pore is denoted as c_p. As the solute diffuses through the pore, its concentration changes and reaches c_{pf} at the pore opening. Then, the solute diffuses through the film around the particle and reaches bulk concentration c_f. The two-film theory describes the solid-fluid interface inside the pore. The overall mass transfer coefficient can be determined from the relationship between the solute concentration in one phase and its equilibrium concentration.

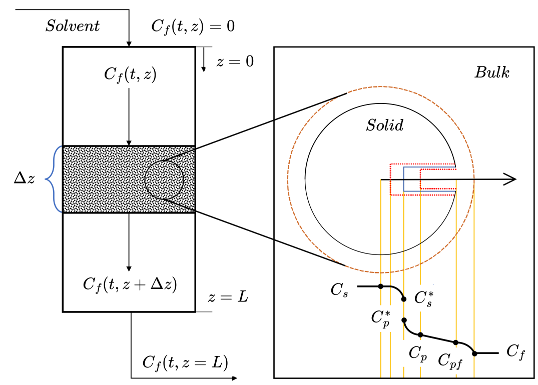

Figure 2: Mass transfer mechanism.

Bulley et al. [12] suggest a process where the driving force for extraction is given by the difference between the concentration of the solute in the bulk, c_f, and in the centre of the pore, c_p^*. The concentration c_p^* is in equilibrium with c_s according to the equilibrium relationship. The rate of extraction is thus $r_e\left(c_f - c_p^*(c_s)\right)$. In contrast, Reverchon [6] proposes a driving force given by the difference between c_s and c_p^*. Concentration c_p^* is determined by the equilibrium relationship with c_f and the extraction rate given by Equation 10:

$$r_e = \frac{D_i}{\mu l^2}\left(c_s - c_p^*\right) \tag{10}$$

where μ is sphericity, l a characteristic dimension of particles that can be defined as $l = r/3$, r is the mean particle radius, ρ_s is the solid density, D_i corresponds to the overall diffusion coefficient and c_P^* is the concentration at the solid-fluid interface (which according to the internal resistance model is supposed to be at equilibrium with the fluid phase).

According to Bulley et al. [12], a linear equilibrium relationship (Equation 11) can be used to find the equilibrium concentration of the solute in the fluid phase c_f^* based on the concentration of the solute in the solid phase c_s:

$$c_f^* = k_p c_s \tag{11}$$

The volumetric partition coefficient k_p acts as an equilibrium constant between the solute concentration in one phase and the corresponding equilibrium concentration at the solid-fluid interphase. According to Spiro and Kandiah [13], k_p can be expressed through the mass partition coefficient k_m:

$$k_m = \frac{k_p \rho_s}{\rho_f} \tag{12}$$

According to Reverchon [6], the kinetic term becomes

$$r_e = -\frac{D_i}{\mu l^2}\left(c_s - \frac{\rho_s c_f}{k_m \rho_f}\right) \tag{13}$$

2.2.5. Uneven solute's distribution in the solid phase

Following the idea of the Broken-and-Intact Cell (BIC) model (Sovova [14]), the internal diffusion coefficient D_i is considered to be a product of the reference value of D_i^R and the exponential decay function γ, as given by Equation 14:

$$D_i = D_i^R \gamma(c_s) = D_i^R \exp\left(\Upsilon\left(1 - \frac{c_s}{c_{s0}}\right)\right) \tag{14}$$

where Υ describes the curvature of the decay function. Equation 15 describes the final form of the kinetic term:

$$r_e = -\frac{D_i^R \gamma}{\mu l^2}\left(c_s - \frac{\rho_s c_f}{k_m \rho_f}\right) \tag{15}$$

The γ function limits the solute's availability in the solid phase. Similarly to the BIC model, the solute is assumed to be contained in the cells, some of which are open because the cell walls were broken by grinding, with the rest remaining intact. The diffusion of the solute from a particle's core takes more time than the diffusion of the solute close to the outer surface. The same idea can be represented by the decaying internal diffusion coefficient, where the decreasing term is a function of the solute concentration in the solid.

Alternatively, the decay function γ can be interpreted by referring to the Shrinking Core model presented by Goto et al. [15], where the particle radius changes as the amount of solute in the solid phase decreases. As the particle size decreases due to dissolution, the diffusion path increases, which makes the diffusion slower and reduces the value of the diffusion coefficient. This analogy can be applied to Equation 14 to justify the application of a varying diffusion coefficient.

2.2.6. Empirical correlations

The empirical correlations for D_i and Υ were derived by article 1 and validated for temperatures between $30-40°C$, pressures between $100-200$ bar, and mass flow rates between $3.33-6.67 \cdot 10^{-5}$ kg/s. Figures 3 and 4 show the results of multiple linear regression applied to solutions of parameter estimation and selected independent variables.

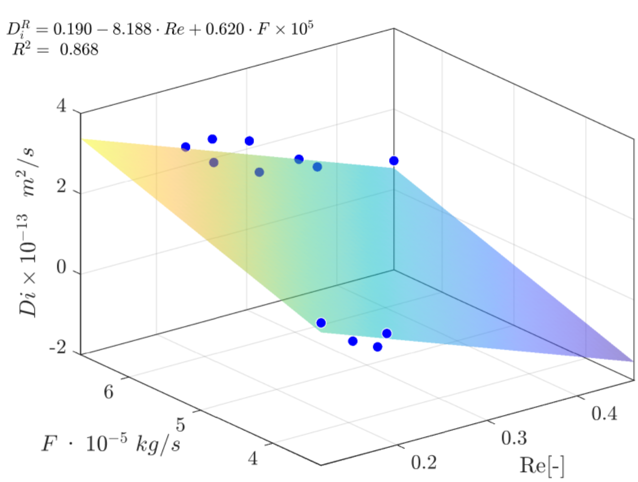

Figure 3: Multiple linear regression $D_i^R = f(Re, F)$

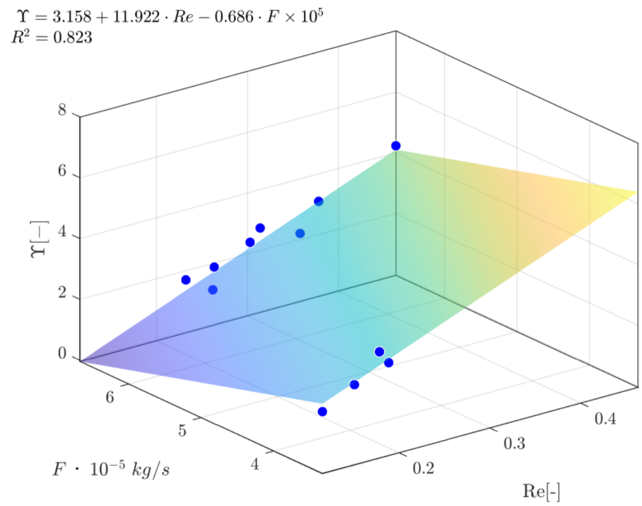

Figure 4: Multiple linear regression $\Upsilon = f(Re, F)$

2.2.7. Heat balance

The heat balance equation describe the evolution of the enthalpy in the system and it is given by Equation 16

$$\frac{\partial\left(\rho_f h A_f\right)}{\partial t} = -\frac{\partial\left(\rho_f h A_f v\right)}{\partial z} + \frac{\partial\left(P A_f\right)}{\partial t} + \frac{\partial}{\partial z}\left(k\frac{\partial T}{\partial z}\right) \tag{16}$$

If the value of enthalpy h is known from the time evolution of the energy equation, and pressure P is known from measurement, then the temperature T can be reconstructed based on the departure function. The departure function is a mathematical function that characterizes the deviation of a thermodynamic property (enthalpy, entropy, and internal energy) of a real substance from that of an ideal gas at the same temperature and pressure. As presented by Gmehling et al. [16], for the Peng-Robinson equation of state, the enthalpy departure function is defined by Equation 17.

$$h - h^{id} = RT\left[T_r(Z-1) - 2.078(1+\kappa)\sqrt{\alpha(T)}\ln\left(\frac{Z+\left(1+\sqrt{2}\right)B}{Z+\left(1-\sqrt{2}\right)B}\right)\right] \tag{17}$$

where α is defined as $\left(1+\kappa\left(1-\sqrt{T_r}\right)\right)^2$, T_r is the reduced temperature, P_r is the reduced pressure, Z is the compressibility factor, κ is a quadratic function of the acentric factor and B is calculated as $0.07780\frac{P_r}{T_r}$.

Equation 17 requires an reference sate, which is assumed to be $T_{ref} = 298.15$ K and $P_{ref} = 1.01325$ bar.

A root-finder can be used to find a value of temperature, which minimizes the difference between the value of enthalpy coming from the heat balance and the departure functions. The root fining procedure to repeated at every time step to find a temperature profile along spatial direction z.

$$\min_T \left(\underbrace{h(t,x)}_{\text{Heat balance}} - \underbrace{h\left(T, P, \rho_f(T,P)\right)}_{\text{Departure function}}\right)^2 \tag{18}$$

2.2.8. Pressure term

As explained in Chapters 2.1, at Low-Mach number conditions, the thermodynamic pressure is nearly constant in space due to the small pressure wave propagation that occurs at the speed of sound. Under such conditions, the term $\partial P/\partial t$ can be approximated by a difference equation, which describes the pressure change in the whole system. The pressure P in the system is considered a state variable, while the pressure in the new time-step P_{in} is considered a control variable.

$$\frac{\partial P}{\partial t} \approx \frac{P_{in} - P}{\Delta t} \tag{19}$$

Such a simplified equation allows for instantaneous pressure change in the system but does not consider a gradual pressure build-up and the effects of pressure losses. In a real system, the dynamics of pressure change would depend on a pump and a back-pressure regulator.

2.2.9. Extraction yield

The process yield is calculated according to Equation 20 as presented by Sovova et al. [17]. The measurement equation evaluates the solute's mass at the extraction unit outlet and sums it up. The integral form of the measurement (Equation 20) can be transformed into the differential form (Equation 21) and augmented with the process model.

$$y = \int_{t_0}^{t_f} \frac{F}{\rho_f} c_f \bigg|_{z=L} dt \tag{20}$$

$$\frac{dy}{dt} = \frac{F}{\rho_f} c_f \bigg|_{z=L} \tag{21}$$

2.2.10. Initial and boundary conditions

It is assumed that the solvent is free of solute at the beginning of the process $c_{f0} = 0$, that all the solid particles have the same initial solute content c_{s0}, and that the system is isothermal, hence the initial state is h_0. The fluid at the inlet is considered not to contain any solute. The initial and boundary conditions are defined as follows:

$$\begin{array}{lll} c_f(t=0,z)=0 & c_s(t=0,z)=c_{s0} & h(t=0,z)=h_0 \\ c_f(t,z=0)=0 & h(t,z=0)=h_{in} & \dfrac{\partial c_f(t,z=L)}{\partial x}=0 \\ \dfrac{\partial h(t,z=L)}{\partial x}=0 & c_s(t,z=\{0,L\})=0 & y(0)=0 \quad P(0)=P_0 \end{array}$$

2.2.11. Discretization methods

The method of lines is used to transform the process model equations into a set of ODEs denoted as $G(x;\Theta)$. The backward finite difference is used to approximate the first-order derivative, while the central difference scheme approximates the second-order derivative z direction. The length of the fixed bed is divided into N_z, i.e. equally distributed points in the z direction. The state-space model after discretization is denoted as x and defined as follows:

$$\dot{x} = \frac{dx}{dt} = \begin{bmatrix} \frac{dc_{f,1}}{dt} \\ \vdots \\ \frac{dc_{f,N_z}}{dt} \\ \hline \frac{dc_{s,1}}{dt} \\ \vdots \\ \frac{dc_{s,N_z}}{dt} \\ \hline \frac{dh_1}{dt} \\ \vdots \\ \frac{dh_{N_z}}{dt} \\ \hline \frac{dP}{dt} \\ \hline \frac{dy}{dt} \end{bmatrix} = \underbrace{\begin{bmatrix} G_1\left(c_f, c_s, h; \Theta\right) \\ \vdots \\ G_{N_z}\left(c_f, c_s, h; \Theta\right) \\ \hline G_{N_z+1}\left(c_f, c_s, h; \Theta\right) \\ \vdots \\ G_{2N_z}\left(c_f, c_s, h; \Theta\right) \\ \hline G_{2N_z+1}\left(c_f, c_s, h; \Theta\right) \\ \vdots \\ G_{3N_z}\left(c_f, c_s, h; \Theta\right) \\ \hline G_{3N_z+1}\left(c_f, c_s, h; \Theta\right) \\ \hline G_{3N_z+2}\left(c_f, c_s, h; \Theta\right) \end{bmatrix}}_{G(x;\Theta)}$$

where $x \in \mathbb{R}^{N_x=3N_z+2}$ and $\Theta \in \mathbb{R}^{N_\Theta=N_\theta+N_u}$, N_θ is the number of parameters, N_u is the number of control variables.

For a derivative to be conservative, it must form a telescoping series. In other words, only the boundary terms should remain after adding all terms coming from the discretization over a grid, and the artificial interior points should be cancelled out. Discretization is applied to the conservative form of the model to ensure mass conservation.

2.3. Local sensitivity analysis

Local derivative-based methods involve taking the total derivative of the state vector x with respect to the parameter space Θ. The set of derivatives, known as sensitivity equations, is integrated simultaneously with the process model. The sensitivity analysis shows how responsive the solution is for changes in the parameter Θ. As discussed by Dickinson and Gelinas [18], the sensitivity analysis can be used to determine the influence of the uncertainty on the solution of the original system. Another application of sensitivity analysis is to distinguish sensitive parameters from insensitive ones, which might be helpful for model reduction. Finally, from a control engineering point of view, the sensitivity analysis allows sorting the control variables with respect to the level of effort required to change the model's output.

Following the work of Maly and Petzold [19], the sensitivity equations can be defined as follow:

$$S(x;\Theta) = \frac{dx}{d\Theta} \tag{22}$$

The new system of equations can be obtained by taking the total derivative of S with respect to time t.

$$\dot{S}(x;\Theta) = \frac{dS(x;\Theta)}{dt} = \frac{d}{dt}\left(\frac{dx}{d\Theta}\right) = \frac{d}{d\Theta}\left(\frac{dx}{dt}\right) = \frac{dG(x;\Theta)}{d\Theta} \tag{23}$$

The sensitivity Equation 24 can be obtained by applying the definition of the total derivative to Equation 23.

$$\frac{dG(x;\Theta)}{d\Theta} = \underbrace{\frac{\partial G(x;\Theta)}{\partial x}}_{\bar{J}_x(x;\Theta)} \underbrace{\frac{\partial x}{\partial \Theta}}_{\bar{S}(x;\Theta)} + \underbrace{\frac{\partial G(x;\Theta)}{\partial \Theta}}_{\bar{J}_\Theta(x;\Theta)} \tag{24}$$

The Jacobian $\bar{J}_x(x;\Theta)$ represents the matrix of equations of size $N_x \times N_x$, where each equation $\bar{J}_x(n_x, n_x)$ is the derivative of $G_{n_x}(x;\Theta)$ with respect to the state variable x_{n_Θ}.

$$\bar{J}_x(x;\Theta) = \begin{pmatrix} \frac{\partial G_1(x;\Theta)}{\partial x_1} & \frac{\partial G_1(x;\Theta)}{\partial x_2} & \cdots & \frac{\partial G_1(x;\Theta)}{\partial x_{N_x}} \\ \frac{\partial G_2(x;\Theta)}{\partial x_1} & \frac{\partial G_2(x;\Theta)}{\partial x_2} & \cdots & \frac{\partial G_2(x;\Theta)}{\partial x_{N_x}} \\ \vdots & \vdots & \ddots & \vdots \\ \frac{\partial G_{N_x}(x;\Theta)}{\partial x_1} & \frac{\partial G_{N_x}(x;\Theta)}{\partial x_2} & \cdots & \frac{\partial G_{N_x}(x;\Theta)}{\partial x_{N_x}} \end{pmatrix} \tag{25}$$

The sensitivity matrix $\bar{S}(x;\Theta)$ represents the matrix of equations of size $N_x \times N_\Theta$, where each entry $\bar{S}(n_x, n_\Theta)$ is the derivative of the state variable x_{n_x} with respect to the parameter Θ_{n_Θ}. Matrix $\bar{J}_x(x;\Theta)$ and $\bar{S}(x;\Theta)$ describe indirect influence of Θ_{n_Θ} on the state space.

$$\bar{S}(x;\Theta) = \begin{pmatrix} \frac{\partial x_1}{\partial \Theta_1} & \frac{\partial x_1}{d\Theta_2} & \cdots & \frac{dx_1}{\partial \Theta_{N_\Theta}} \\ \frac{\partial x_2}{\partial \Theta_1} & \frac{\partial x_2}{d\Theta_2} & \cdots & \frac{dx_2}{\partial \Theta_{N_\Theta}} \\ \vdots & \vdots & \ddots & \vdots \\ \frac{\partial x_{N_x}}{\partial \Theta_1} & \frac{\partial x_{N_x}}{d\Theta_2} & \cdots & \frac{\partial x_{N_x}}{d\Theta_{N_\Theta}} \end{pmatrix} \tag{26}$$

The Jacobian $\bar{J}_\Theta(x;\Theta)$ represents the matrix of equations of size $N_x \times N_\Theta$, where each subequation $\bar{J}_\Theta(n_x, n_\Theta)$ is the partial derivative of the process model equation G_{n_x} with respect to the parameter Θ_{n_Θ}. $\bar{J}_\Theta(n_x, n_\Theta)$ defines direct effect of Θ_{n_Θ} on the state space.

$$\bar{J}_\Theta(x;\Theta) = \begin{pmatrix} \frac{\partial G_1(x;\Theta)}{\partial \Theta_1} & \frac{\partial G_1(x;\Theta)}{\partial \Theta_2} & \cdots & \frac{\partial G_1(x;\Theta)}{\partial \Theta_{N_\Theta}} \\ \frac{\partial G_2(x;\Theta)}{\partial \Theta_1} & \frac{\partial G_2(x;\Theta)}{\partial \Theta_2} & \cdots & \frac{\partial G_2(x;\Theta)}{\partial \Theta_{N_\Theta}} \\ \vdots & \vdots & \ddots & \vdots \\ \frac{\partial G_{N_x}(x;\Theta)}{\partial \Theta_1} & \frac{\partial G_{N_x}(x;\Theta)}{\partial \Theta_2} & \cdots & \frac{\partial G_{N_x}(x;\Theta)}{\partial \Theta_{N_\Theta}} \end{pmatrix} \tag{27}$$

The augmented system containing the original set of equations $G(x;\Theta)$ and sensitivity equations can be formulated as $\mathbf{G}(x;\Theta)$. The size of $\mathbf{G}(x;\Theta)$ is equal to $N_s = N_x(N_\Theta + 1)$.

$$\mathbf{G}(x;\Theta) = \begin{bmatrix} G(x;\Theta) \\ \bar{J}_x(x;\Theta)\bar{S}(x;\Theta) + \bar{J}_\Theta(x;\Theta) \end{bmatrix} \tag{28}$$

The initial conditions are described as

$$\mathbf{G}\left(x(t_0);\Theta\right) = \begin{bmatrix} x(t_0), & \frac{\mathrm{d}x(t_0)}{d\Theta_1}, & \cdots, & \frac{dx(t_0)}{d\Theta_{N_\Theta}} \end{bmatrix}^\top = \tag{29}$$

$$= \begin{bmatrix} x_0, & 0, & \cdots, & 0 \end{bmatrix}^\top \tag{30}$$

The sensitivity analysis of the output function can be performed with respect to parameters Θ. The output function $g(x)$ returns y. By taking a total derivative of y with respect to Θ, the new sensitivity equation can be found.

$$\frac{dy}{d\Theta} = \frac{dg(x)}{d\Theta} = \frac{\partial g(x)}{\partial x}\frac{\partial x}{\partial \Theta} + \frac{\partial g(x)}{\partial \Theta} \tag{31}$$

3. Results

The details of the process model and parameters are delivered in article 1. The process model was validated under the following range of operating conditions: temperatures between $30 - 40°C$, pressures between $100 - 200$ bar, and mass flow rates between $3.33 - 6.67 \cdot 10^{-5}$ kg/s. The sensitivity analysis is performed at the midpoint of the validated range: $35°C$, 150 bar and $5 \cdot 10^{-5}$ kg/s. This study examines the impact of pressure change on the state space and extraction yield through the local sensitivity analysis. The local sensitivity analysis results can be interpreted as the system's response to an infinitesimal deviation in pressure.

As discussed in Chapter 2.1, a small pressure wave propagates at the speed of sound relative to the flow. When the flow velocity is relatively low, pressure changes are hydrodynamic (resulting from velocity motion) rather than thermodynamic. The Low Mach number assumption allows for the instant propagation of thermodynamic pressure throughout the system, enabling a single pressure value to be considered for the entire system. In response to a pressure change, the energy equation experiences a simultaneous deviation across the entire spatial domain. This pressure change impacts the fluid's temperature within the computational domain, while boundary values are constrained by conditions specified at the domain's extremes. Dirichlet boundary conditions impose a fixed temperature value at the inlet, creating a thermal gradient that propagates through the system. Conversely, Neumann boundary conditions specify the heat flux at the boundaries. In this study, zero Neumann boundary conditions were applied to ensure that the temperatures at the inlet, outlet, and within the extractor vary uniformly in response to the pressure change.

Figure 5 illustrates the sensitivity of solute concentration in the solid phase to pressure changes. As discussed in Chapter 2.2.1, the velocity of a fluid is inversely proportional to its density, indicating that increased pressure reduces the fluid's velocity. This results in an extended residence time, allowing for longer interaction between the solute and solvent. Initially, the extraction process operates in the kinetic-controlled regime, where the concentration gradient is high, and solute solubility is the limiting factor. As noted in [article 1], the system is considered far from saturation, which explains the low initial system response. This low initial response was also observed in the sensitivity analysis by Fiori et al. [7]. The system's response becomes more pronounced as the concentration gradient decreases and the extraction shifts from the kinetic-controlled to the diffusion-controlled regime. The negative sensitivity indicates a faster solute loss from the solid phase, corresponding to enhanced mass transfer. Over time, as the amount of solute decreases, it becomes a limiting factor, reducing the effect of pressure changes on the system. Eventually, the sensitivities approach zero asymptotically as the solute is washed out from the bed.

Figure 6 illustrates the sensitivity of solute concentration in the fluid phase to pressure changes. Compared to Figure 5, the dynamic behaviour of fluid phase sensitivities is more apparent. Due to advection, the sensitivities move

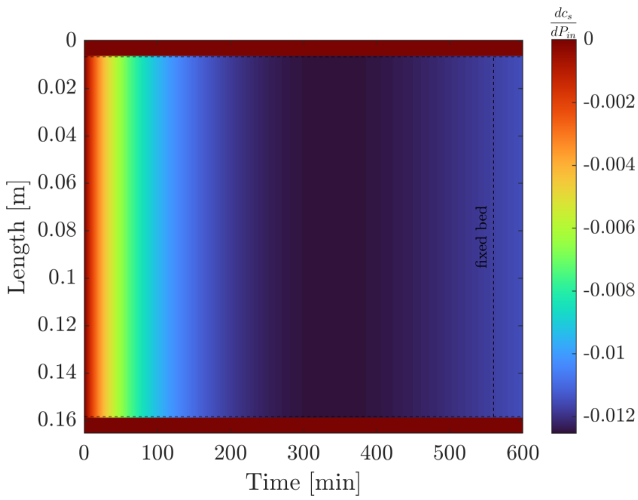

Figure 5: The effect of P_{in} change on C_s

through the system similarly to the solute in the fluid phase. Initially, the system response is low despite the pressure increase improving mass transfer, reflecting the previously discussed idle period. As the process continues, the sensitivities increase, indicating faster solute loss from the solid phase. The positive sensitivities show that more solute is being transported from the solid particles to the fluid. When the solute in the solid phase becomes a limiting factor, the extraction rate slows, and sensitivities decline to negative values, eventually approaching zero asymptotically.

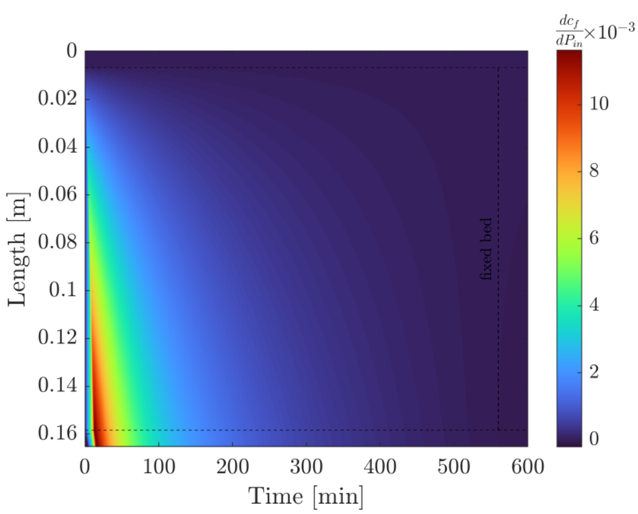

Figure 6: The effect of P_{in} change on C_f

Figure 7 show how sensitive the extraction yield is to pressure changes over an extended period for various pressure values. Initially, all sensitivity curves remain nearly flat, indicating a delayed response in the system. Due to the reduced fluid velocity, the solute reaches the extractor's outlet later, causing minor negative sensitivities to appear. Once the solute exits the extractor, the sensitivity curves rise rapidly. Positive yield sensitivities indicate improved process efficiency and enhanced mass transfer. The peak in $\frac{dy}{dP_{in}}$ represents the point of greatest deviation from the original system. Eventually, the sensitivities decline and converge towards zero as the concentration gradient becomes a limiting factor, reducing the impact of enhanced mass transfer.

As presented in Figure 7, higher sensitivities are observed for the low-pressure system. At lower pressures, the supercritical fluid has lower density and solvating power, which results in less efficient extraction as shown by data given in article 1. Small changes in pressure at low pressures can significantly impact the solute's solubility and, consequently, the extraction yield. Moreover, near the critical point, small changes in pressure can lead to significant changes in the physical properties of the supercritical fluid, such as density and viscosity. These changes can strongly affect the solute's solubility and the mass transfer rates, resulting in higher sensitivity at lower pressures where the system operates closer to the critical point.

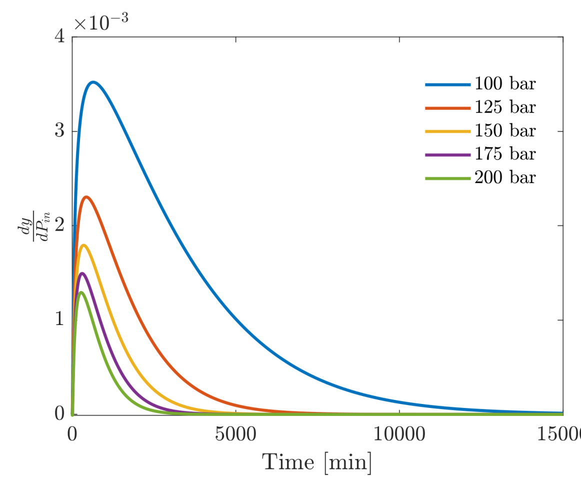

Figure 7: The effect of P_{in} change on $y(t)$

4. Conclusions

Sensitivity analysis is a tool used to understand how model parameters affect its output. The presented formulation involves derivative-based local sensitivity analysis of the model solution with respect to selected parameters and controls. This work implemented the automatic differentiation to derive the sensitivity equations. The local sensitivity analysis techniques consider only a small region of parameter space, and the conclusions derived from such an analysis are limited to local conditions. In the case of dynamical systems, local sensitivity analysis provides a time series describing how that dependency evolves.

The local sensitivity analysis can be performed with respect to any model parameter, but this work focuses on the effect of pressure increase. At selected operating conditions ($35°C$, 150 bar and $5 \cdot 10^{-5}$ kg/s), the pressure increase enhances the mass transfer, which leads to faster loss of solute from particles and consequently to negative sensitivities in the solid phase. Analogously, the sensitivities in the fluid phase are characterised by positive deviations, which indicates that more solute is transported to the fluid phase. As a result, the extraction yield is improved and characterised by positive sensitivities. As the results of the local sensitivity analysis depends on the operating point, the analysis was repeated at different nominal pressures. It can be observed that system responses at low-pressures are stronger than at high-pressures. This behaviour can be explained by more rapid changes of the solvent properties close to the critical point and lower process efficiency at low-pressure.

Local sensitivity analysis can provide valuable information by identifying which parameters are influential and how these influence changes over time. Sensitivity analysis can highlight discrepancies between model predictions and actual experimental results. Identifying unexpected relationships or non-linearities can prompt further investigation and refinement of the process model. Sensitivity analysis can inform the design of future experiments by indicating which parameters should be varied and monitored.

References

[1] O. Singh, Z. Khanam, N. Misraand, and M.K. Srivastava. Chamomile (matricaria chamomilla l.): An overview. Pharmacognosy Reviews, 5 (9):82, 2011. ISSN 0973-7847. doi: 10.4103/0973-7847.79103.

[2] J. Srivastava. Extraction, characterization, stability and biological activity of flavonoids isolated from chamomile flowers. Molecular and Cellular Pharmacology, 1(3):138–147, August 2009. ISSN 1938-1247. doi: 10.4255/mcpharmacol.09.18.

[3] A. Orav, A. Raal, and E. Arak. Content and composition of the essential oil ofchamomilla recutita(l.) rauschert from some european countries. Natural Product Research, 24(1):48–55, January 2010. ISSN 1478-6427. doi: 10.1080/14786410802560690.

[4] E. Reverchon, G. Donsi, and L.S. Osseo. Modeling of supercritical fluid extraction from herbaceous matrices. Industrial & Engineering Chemistry Research, 32(11):2721–2726, nov 1993. doi: 10.1021/ie00023a039.

[5] H. Sovova. Rate of the vegetable oil extraction with supercritical co2. modelling of extraction curves. Chemical Engineering Science, 49 (3):409–414, 1994. doi: 10.1016/0009-2509(94)87012-8.

[6] E. Reverchon. Mathematical modeling of supercritical extraction of sage oil. AIChE Journal, 42(6):1765–1771, June 1996. ISSN 1547-5905. doi: 10.1002/aic.690420627.

[7] L. Fiori, D. Calcagno, and P. Costa. Sensitivity analysis and operative conditions of a supercritical fluid extractor. The Journal of Supercritical Fluids, 41(1):31–42, may 2007. doi: 10.1016/j.supflu.2006.09.005.

[8] M.M. Santos, E.A. Boss, and R. Maciel Filho. Supercritical extraction of oleaginous: parametric sensitivity analysis. Brazilian Journal of Chemical Engineering, 17(47):713–720, December 2000. ISSN 0104-6632. doi: 10.1590/s0104-66322000000400035.

[9] T. Hatami and O.N. Ciftci. Techno-economic sensitivity assessment for supercritical co2 extraction of lycopene from tomato processing waste. The Journal of Supercritical Fluids, 204:106109, January 2024. ISSN 0896-8446. doi: 10.1016/j.supflu.2023.106109.

[10] J. D. Jr Anderson. Computational fluid dynamics the basic with applications. McGraw-Hill, 1995. ISBN 9780071132107.

[11] J. D. Jr Anderson. Fundamentals of Aerodynamics. McGraw-Hill Education, 2023. ISBN 9781264151929.

[12] N. R. Bulley, M. Fattori, A. Meisen, and L. Moyls. Supercritical fluid extraction of vegetable oil seeds. Journal of the American Oil Chemists' Society, 61(8):1362–1365, aug 1984. doi: 10.1007/bf02542243.

[13] M. Spiro and M. Kandiah. Extraction of ginger rhizome: partition constants and other equilibrium properties in organic solvents and in supercritical carbon dioxide. International Journal of Food Science & Technology, 25(5):566–575, jun 2007. doi: 10.1111/j.1365-2621.1990.tb01116.x.

[14] H. Sovova. Broken-and-intact cell model for supercritical fluid extraction: Its origin and limits. The Journal of Supercritical Fluids, 129:3–8, nov 2017. doi: 10.1016/j.supflu.2017.02.014.

[15] M. Goto, B.C. Roy, and T. Hirose. Shrinking-core leaching model for supercritical-fluid extraction. The Journal of Supercritical Fluids, 9 (2):128–133, jun 1996. doi: 10.1016/s0896-8446(96)90009-1.

[16] J. Gmehling, M. Kleiber, B. Kolbe, and J. Rarey. Chemical Thermodynamics for Process Simulation. Wiley, mar 2019. doi: 10.1002/9783527809479.

[17] H. Sovova, R. Komers, J. Kucuera, and J. Jezu. Supercritical carbon dioxide extraction of caraway essential oil. Chemical Engineering Science, 49(15):2499–2505, aug 1994. doi: 10.1016/0009-2509(94) e0058-x.

[18] R.P. Dickinson and R. J. Gelinas. Sensitivity analysis of ordinary differential equation systems—a direct method. Journal of Computational Physics, 21(2):123–143, jun 1976. doi: 10.1016/0021-9991(76)90007-3.

[19] T. Maly and L.R. Petzold. Numerical methods and software for sensitivity analysis of differential-algebraic systems. Applied Numerical Mathematics, 20(1-2):57–79, feb 1996. doi: 10.1016/0168-9274(95) 00117-4.